Multimode Radiative Transfer in Finite Optical Media. II: Solutions

GRAEME L. STEPHENS

Division of Atmospheric Physics, CSIRO, Aspendale, Victoria, Australia

RUDOLPH W. PREISENDORFER

Pacific Marine Environmental Laboratory, NOAA, Seattle, WA 98195

(Manuscript received 13 May 1983, in final form 7 November 1983)

ABSTRACT

This paper extends the theoretical developments of Part I to illustrate the power of the method in solving multiple scattering problems with sources that result from i) the single scatter of a collimated beam of solar radiation that is directly transmitted to a given point in the medium and ii) thermal emission. These source terms are derived in the multimode context and solutions are presented to illustrate the effects of sun angle and infrared emission on the radiance and irradiance fields that emerge from hypothetical box shaped clouds. The results reiterate the earlier findings that the sides of clouds play an important role in the exchange of radiative energy between the cloud and its environment. The total infrared emission by cuboidal clouds, for example, is shown to be substantially larger than the emission from plane parallel clouds as a result of this additional exchange of radiant energy.

The results presented in the paper, including the comparisons with available Monte Carlo calculations show the multimode approach to be a viable, accurate and computationally efficient method of solving the general problem of anisotropic scattering in horizontally finite optical media.

1. Introduction

In Preisendorfer and Stephens (1984), hereafter referred to as Part 1, the radiative transfer equation was transformed using two-dimensional Fourier series to solve the problem of radiative transfer in a laterally finite medium. Solutions were presented for the relatively simple case for which it was assumed that there were no sources of radiation in a medium which was illuminated only on its upper face. The advantage of this multimode approach is that the new equation includes the explicit effects of the lateral sides of the medium but yet it is in a form that is exactly analogous to the plane-parallel equation.

This paper extends the concepts of Part 1 to address three issues that are commonly encountered in problems of atmospheric radiation; namely i) to include the effects of variable sun angle, ii) to include the effects of thermal emission, and iii) to assess the effects of diffuse incident radiation to the overall solutions. The major emphasis of the paper is therefore to extend Part 1 in such a way that the multimode method can be fruitfully applied to a variety of solar and IR atmospheric radiation problems.

Section 2 briefly outlines the essential features of the multimode procedure while a simple transformation is described in Section 3 that decouples the geometric modes from the set of differential equations and the solution reduces to a simple combination of equivalent plane parallel solutions. In Section 4, the direct (unscattered) radiation problem is solved in the multimode context. Section 5 presents the multimode equation for diffuse radiance with the "direct beam" source term together with a brief outline of scattering matrices and vectors required for use in appropriate doubling algorithms which are used to solve the equations.

Section 6 describes the thermal emission source term together with a simplified diffuse incident radiance term. Some example solutions of the multimode equation with these two source terms are presented in Section 7.

2. The radiative transfer equation in the multimode setting

The general radiance function on a three-dimensional box shaped medium, similar to that illustrated in Fig. 1 of Part 1, is a function of three location variables (u, v and y) and the directional variable ξ. The essence of the multimode procedure is to remove from the radiative transfer equation the horizontal dependencies u and v by using radiance amplitudes in a two dimensional Fourier series

$$N(u, v, y, \xi) = \sum_{w=0}^{\infty} \sum_{l=0}^{\infty} \hat{N}(l, w, y, \xi) \cos \frac{l\pi u}{L} \cos \frac{w\pi v}{W}, \quad (1)$$

where $\hat{N}(l, w, y, \xi)$, for fixed integers l and w (length and width wave numbers respectively) are the multimode amplitudes which are functions of y and ξ. The amplitudes are obtained from

$$\hat{N}(u, v, y, \xi) = \frac{4}{L_l W_w} \int_0^W \int_0^L N(u, v, y, \xi) \times \cos \frac{l\pi u}{L} \cos \frac{w\pi v}{W} \, dudv, \quad (2)$$

where L_l, W_w, L and W and other symbols are defined in Part 1. Thus the *radiance amplitudes* for a given set of l and w are analogous to the *radiance function* of the more classical plane-parallel problem and both of these are functions only of the vertical (y) and directional (ξ) coordinates. The latter coordinate can be specified in terms of the zenith (θ or $\mu = \cos\theta$) and azimuth angle ϕ. The amplitude function $\hat{N}(l, w, y, \mu, \phi)$ can be further expressed as a function of an azimuthal mode by use of the Fourier series

$$\hat{N}(l, w, y, \mu, a) = \sum_{a=0}^{\infty} \hat{N}_1(l, w, y, \mu, a) \cos a\phi + \hat{N}_2(l, w, y, \mu, a) \sin a\phi, \quad (3)$$

where now each amplitude pair $\hat{N}_j(l, w, y, \mu, a)$ with $j = 1, 2$ for fixed l, w and a are functions only of two variables; depth and the cosine factor μ.

In Part 1, we applied the multimode representation of radiance to the radiative transfer equation to derive the following vector equation

$$\mu \frac{d\mathbf{N}}{dy} = -\left(\alpha \mathbf{I} + \eta \frac{\mathbf{S} + \mathbf{B}}{\pi}\right)\mathbf{N} + \pi s \int_{-1}^{+1} \mathbf{P}\mathbf{N} d\mu' + \underline{\mathbf{N}_{si}} + \mathbf{N}_\epsilon \quad (4)$$

where $\mathbf{N}$ is the vector of amplitudes whose transpose is

$$\mathbf{N} = [\hat{N}(l, w, y, \mu, a); l, w, a = 0, 1, 2 \cdots]^{\mathrm{T}} \quad (5)$$

while $\mathbf{I}$ is an identity tensor, $\mathbf{P}$ is a scattering tensor defined from the scattering phase function, $\mathbf{S}$ is an emergent tensor, $\mathbf{B}$ is a divergence tensor and $\mathbf{N}_{si}$ is a vector associated with the incident illumination on the sides of the medium. In (4), η is the sine of the zenith angle, α the volume extinction coefficient and s is the scattering coefficient. The source vector $\mathbf{N}_\epsilon$ is transformed to the multimode setting and is derived below for the case of thermal emission within the medium and the case of diffuse radiance that arises from the single scatter of the directly transmitted solar beam. The form of (4) for $\mathbf{N}$ is directly analogous to the radiative transfer equation for radiance (N) in a plane-parallel medium with the addition of the two underlined terms. The interpretation of these terms is discussed more fully in Part 1 but it suffices to say that they refer to apparent sources and sinks of radiation resulting from the gain and loss of radiation through the lateral sides of the medium.

3. The general solution of the multimode radiative transfer equation: Principle modes

The solution of the classical plane-parallel radiative transfer equation is generally carried out by replacement of the integral term with a suitable quadrature formula thus producing a system of coupled differential equations. For the multimode transfer problem, one again establishes a system of coupled differential equations. This coupling arises not only through the discretization of the angular integral but also through the interactions of various geometric modes. While these interactions produce a much larger set of coupled differential equations (the price one pays for the increased complexity of the radiance function in the three dimensional setting), the equations for the modal amplitudes $\hat{N}(l, w, y, \mu, a)$ are formally equivalent to the matrix version of the equation of transfer for a plane-parallel medium. In Part 1 we presented the general solution to, and the interaction form of, this large system of coupled differential equations.

It was mentioned in Part 1 that even for a relatively small number of geometric modes and quadrature angles, the general solution became unwieldy and involved operations on very large matrices. However, the solution is considerably simplified if the geometric modes of the emergent radiance term (i.e., $-\eta/\pi[(\mathbf{S} + \mathbf{B})\mathbf{N}]$, and the geometric modes of the path function (i.e., $\int \mathbf{P}\mathbf{N} d\mu'$) are decoupled. This can be achieved by diagonalizing the combined tensor ($\mathbf{S} + \mathbf{B}$) while simultaneously preserving the diagonal form of $\mathbf{P}$. Unfortunately, the diagonalization cannot be achieved in general without placing certain restrictions on $\mathbf{P}$. From Eq. (34) of Part 1, the phase function is diagonal, i.e.

$$\mathbf{P} = \begin{pmatrix} 1 + \delta_a & 0 \\ 0 & 1 \end{pmatrix} p(\mu, \mu', a), \quad (6)$$

where δ_a is Kronecker's delta (see Appendix of Part 1).

For illustrative purposes only, we will consider only the azimuthally averaged solutions (i.e. $a = 0$) (or equivalently we will assume that the solutions for the general azimuthal mode are not greatly influenced by the azimuthal asymmetries in $\mathbf{P}$). If we make these assumptions, it follows that

$$\mathbf{P} = \mathbf{I}\bar{p}(\mu, \mu'), \quad (7)$$

where $\bar{p}(\mu, \mu')$ is the scalar value of the azimuthally averaged phase function. This assumption is probably not too restrictive given that clouds are generally optically thick and radiation within such media is transported by a simple diffusion mode which is approximately isotropic (Van de Hulst, 1980). This point is

borne out in the comparisons presented below between multimode solutions and Monte Carlo solutions.

Given (7), the problem of decoupling the radiative transfer equation (4) from its geometric modes requires the diagonalization of the $\mathbf{S} + \mathbf{B}$ tensor via

$$\mathbb{D} = \mathbb{E}(\mathbf{S} + \mathbf{B})\mathbb{E}^{-1}. \tag{8}$$

Here $\mathbb{D}$ is the required diagonal form of $(\mathbf{S} + \mathbf{B})$ and $\mathbb{E}$ is the associated eigenfunction tensor.

The multimode radiative transfer equation (4) can then be transformed to

$$\mu \frac{d\mathbb{N}^+}{dy} = -\left[\alpha\mathbb{I} + \frac{\eta}{\pi}\mathbb{D}\right]\mathbb{N}^+ + \pi s \int_{-1}^{+1} \bar{p}(\mu, \mu')\mathbb{N}^+ d\mu' + \mathbb{N}_{si}^+ + \mathbb{N}_\epsilon^+ \tag{9}$$

with

$$\mathbb{N}^+ = \mathbb{E}^{-1}\mathbb{N}. \tag{10}$$

The radiative transfer equation in the form described by (9) can be solved directly for each of the principle modes of $\mathbb{N}^+$. The radiance amplitude vectors $\mathbb{N}$ are retrieved by the transformation

$$\mathbb{N} = \mathbb{E}\mathbb{N}^+, \tag{11}$$

and the radiance function $N(u, v, y, \mu, \phi)$ is finally obtained by applying the analysis formulas (1) and (3) to obtain the radiance fields within the medium.

4. Solution of the directly transmitted radiances

For solar radiation problems, it is desirable to provide flexibility to the solution of (9) by allowing incident illumination at angles other than those specified by the quadrature angles. This can be achieved first by separating the radiance field into its diffuse and direct components and then by incorporating the direct beam solution in the radiative transfer equation for diffuse radiance by way of a source term. In the plane parallel medium the direct beam solution is provided by the simple Beer's relation. Unfortunately, the direct beam solution is far more involved in the multimode setting. The purpose of this section is to provide this solution and to couple it to the general multimode radiative transfer equation.

a. Analytic solution

Consider a cloud shown schematically in Fig. 1 with given optical dimensions (αL, αW, αH) which is externally illuminated by a unidirectional beam of radiance ($F_0/4\pi$) in the directions θ_0 and ϕ_0. In the following, we set $\phi_0 = 0$ and, since the azimuth is measured from the positive u axis, only the top and one of the vertical faces (the west face, see Fig. 3 of Part 1 for reference) of the box are illuminated uniformly by $F_0/4\pi$. The solutions for other cases are straight forward and can be developed in a similar manner.

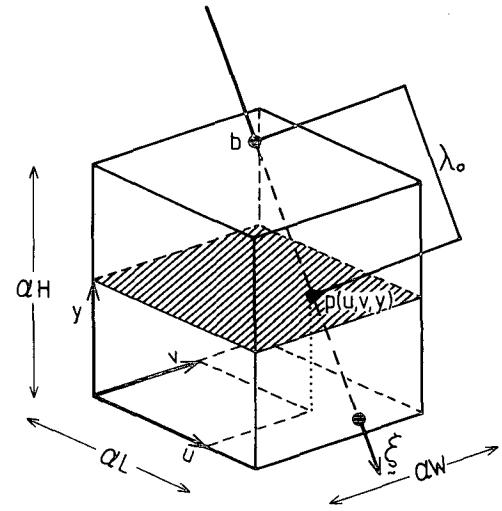

FIG. 1. Schematic view of the directly transmitted beam through the optical medium $X(a, b)$.

The directly transmitted radiance to a point ($p = u, v, y$) in the box along some general direction defined by ξ can be written simply as

$$N_0(u, v, y, \xi) = \frac{F_0}{4\pi} \exp\left\{-\int_0^{\lambda_0} \alpha d\lambda\right\}, \tag{12}$$

where λ_0 is the distance from b, the point of entry of the beam on the face of the box to p along the direction ξ. Given $\phi_0 = 0$, $\mu_0 = \cos\theta_0$, $\eta_0 = \sin\theta_0$ and that α is independent of λ, then

$$N_0(u, v, y, \mu_0, \phi_0) = \frac{F_0}{4\pi} \exp(-\alpha\lambda_0), \tag{13}$$

where

$$\left.\begin{aligned} \lambda_0 &= \frac{(H - y)}{\mu_0}, \quad u \geq u^* \\ \lambda_0 &= \frac{u}{\eta_0}, \quad u \leq u^* \end{aligned}\right\}$$

for

$$u^* = \frac{(H - y)}{\eta_0}.$$

The solution given by (13) applies to two distinctly different regions within the medium where the variation of radiance with depth is different for each region. These two regions are illustrated in Fig. 2 where a vertical slice through the cloud parallel to the u axis is shown. For radiation incident on the top and side face(s) of the cloud at an angle θ_0, the behaviour of N_0 with variations in y can be ascertained by travelling along the vertical line shown in Fig. 2. This line corresponds to a set of points with the same u and v coordinates. The radiance in the shaded region is a result of the transmission through the top of the cloud and drops off exponentially with depth (i.e., with

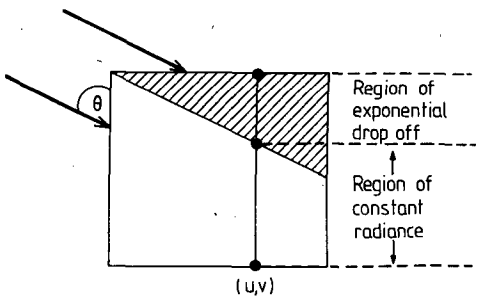

FIG. 2. Schematic view of the different regions that result from the direct transmission of irradiance that illuminates both the top and side of $X(a, b)$.

$H - y$) to some finite depth defined at $y^* = u^*\eta_0$. Below this point (i.e., $y < y^*$), the radiance remains constant with depth. In this constant-with-depth region, the radiance results from the direct transmission of the illumination on the side of the cloud.

b. The multimode solution

The multimode amplitudes of the directly transmitted radiance function $N_0(u, v, y, \xi)$ can be obtained by substituting (12) into (2) to derive the modal amplitude of the radiance function $N_0(u, v, y, \mu_0, \phi_0 = 0)$. That is

$$\hat{N}_0(l, w, y, \mu_0, \phi_0 = 0) = \frac{2F_0}{4\pi}\frac{\delta_w}{L_l}\left[\int_0^{u^*} e^{-\alpha u/\eta_0} \times \cos\frac{l\pi u}{L}\,du + \int_{u^*}^{L} e^{-\alpha y/\mu_0}\cos\frac{l\pi u}{L}\,du\right]. \quad (14)$$

The solution of (14) follows as

$$\hat{N}_0(l, w, y, \mu_0, \phi_0 = 0) = \frac{F_0}{4\pi}\frac{\delta_w}{L}[(L - u')e^{-\alpha y/\mu_0} + \eta_0(1 - e^{-\alpha u'/\eta_0})/\alpha], \quad (15)$$

where $u' = \min(u^*, L)$ and $l = 0$. For all other modes (i.e., $l > 0$)

$$\hat{N}_0(l > 0, w, y, \mu_0, 0) = \frac{F_0}{4\pi}\frac{\delta_w}{L}\left\{\left[e^{-\alpha u'/\mu_0}\left(l'\sin\gamma - \frac{\alpha}{\eta_0}\cos\gamma\right) + \frac{\alpha}{\eta_0}\right]\beta^{-1} - \frac{1}{l'}e^{-\alpha y/\mu_0}\sin\gamma\right\} \quad (16)$$

where $l' = l\pi/L$, $\beta = \alpha^2/\eta_0^2 + l'^2$, $\gamma = l'u'$.

Figure 3 presents the multimode and analytic solutions (15), (16) and (13), respectively, for the irradiance distribution at cloud base as a function of horizontal position (shown as fractions of L) for different values of NL used to truncate the series in (1). The calculations were performed for a cuboidal cloud with optical dimensions (5, 5, 5) which was illuminated on the top and west faces of the cloud by a collimated beam at a zenith angle of 60°. It is apparent from the example presented here that the irradiance distribution is generally well handled as a function of u even for a small number of terms taken to represent the summation in (1).

The comparisons shown on Fig. 3 illustrate an important point with regard to the number of l modes that are required to represent the distribution of N_0 within the medium. It is evident from Fig. 3 that matching the incoming boundary radiation on the cloud face at $u = 0$ requires more terms than for either an accurate representation on the interior of the cloud or for the application of (15) or (16) as a source of diffuse radiation. This latter point is supported by studying the radiance source vectors derived in the Appendix. Inspection of (A15) reveals that the source vectors contain a $1/l^2$ factor in addition to the factors apparent in (16). Thus only a small number of l modes are required to represent the source functions associated with the direct beam solution (16).

5. The multimode equation for diffuse radiation

The radiance amplitudes $\hat{N}(l, w, y, \mu, a)$ can be divided into their diffuse and direct components in the same manner as for the radiance function $N(u, v, y, \mu, \phi)$, that is

$$\mathbf{N} = \mathbf{N}^* + \mathbf{N}_0, \quad (17)$$

where $\mathbf{N}^*$ and $\mathbf{N}_0$ are the amplitude vectors associated with the diffuse and direct (i.e., unscattered) radiance

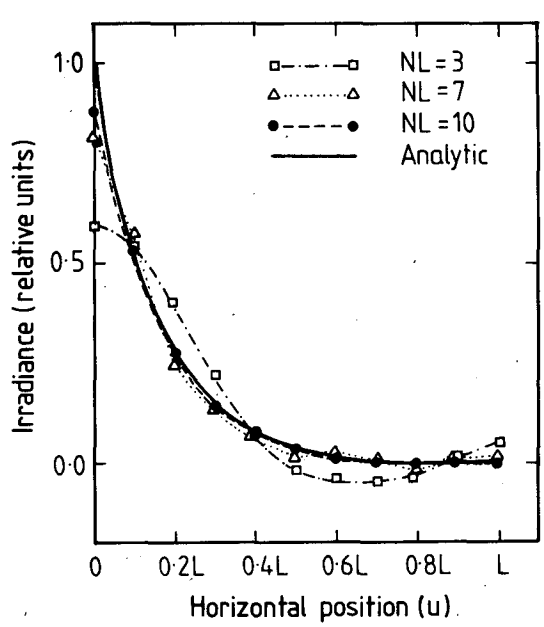

FIG. 3. Cloud base irradiance distribution as a function of horizontal variable u for $\mu_0 = 0.5$ and $\phi_0 = 0$. The multimode solutions are shown for various orders of truncation (NL).

fields respectively. The vector $\mathbb{N}_0$ is defined according to (5) with the amplitudes given by (15) and (16) for $l = 0$ and $l > 0$ respectively. The governing equation for the diffuse amplitude vector follows from (9) as

$$\mu \frac{d\mathbb{N}^{*+}}{dy} = -\left[\alpha\mathbb{I} + \frac{\eta}{\underline{\pi}}\mathbb{D}\right]\mathbb{N}^{*+} + \pi s \int_{-1}^{+1} \tilde{p}(\mu, \mu')[\mathbb{N}^{*+} + \delta_{\mu_0}\mathbb{N}_0^+]d\mu' + \frac{\mathbb{N}_{si}^*}{\underline{\mathbb{B}}}, \quad (18)$$

where the superscripts "+" again remind us that all quantities are transformed according to (10). Note that (18) refers to a collimated source of radiance, represented by the vector $\delta_{\mu_0}\mathbb{N}_0^+$, along the direction cosine μ_0. This term, as described more fully below, therefore represents a source of diffuse radiance (represented as $\mathbb{N}_\epsilon^{*+}$). Thus the solution of (18) for $\mathbb{N}^{*+}$ is formally equivalent to the solution of the more familiar plane parallel equation with the exception of the underlined terms (A and B) and the solution is sought for each of the principle modes.

a. Construction of the reflection and transmission matrices

The construction of the reflection and transmission matrices associated with (18) follows the standard plane-parallel procedures with the exception of term A. The modification of the transmission matrix to include this term is trivial [a similar modification was described in Part 1, see Eq. (39)]. The general derivation of these scattering matrices for the plane parallel solution can be found in Wiscombe (1976a,b). The matrices in the present multimode context are

$$\left.\begin{aligned} \mathbb{t}^+(y) &= -[\mathbb{I} + \mathbb{L}\mathbb{D}/\pi\alpha - \pi\omega_0\mathbb{C}\mathbb{P}]\mathbb{M}^{-1} \\ \rho^+(y) &= \pi\omega_0\mathbb{C}\mathbb{P}^-\mathbb{M}^{-1} \end{aligned}\right\}, \quad (19)$$

respectively, for transmission and reflection where the superscript (+) on ρ and $\mathbb{t}$ is again used for the transformation (10).

Both $\mathbb{t}^+(y)$ and $\rho^+(y)$ are square matrices of order m (the number of quadrature angles employed to approximate the integral term). $\mathbb{L}$ and $\mathbb{D}$ are diagonal matrices; the diagonal elements of $\mathbb{L}$ correspond to the sine factor η_i while $\mathbb{D}$ is defined by (8). All other matrices are defined according to the normal plane-parallel context, i.e., $\mathbb{C}$ and $\mathbb{M}$ are diagonal with elements given by the quadrature weights c_i and the abscissae μ_i respectively while $\mathbb{P}$ and $\mathbb{P}^-$ represent the forward and backward scattering matrices defined from the scattering phase function and $\mathbb{I}$ is the identity matrix.

b. Construction of the source vectors

The source of diffuse radiance, in the context described above, can be defined by the following vector

$$\mathbb{N}_\epsilon^{*+} = \pi\omega_0\bar{p}(\mu, \mu_0)\mathbb{N}_0^+. \quad (20)$$

Doubling algorithms have been developed for source functions which possess a depth dependence that is either linear, quadratic or simple exponential (e.g., Wiscombe, 1976a,b). The problem that arises in employing source terms which are described by (15) and (16) are substituted in (20) is that the depth dependence is not a simple exponential and suitable algorithms are required to render the solutions to a doubling form. These algorithms are described in the Appendix.

6. The multimode radiative transfer equation with thermal emission

a. Source term $\mathbb{N}_\epsilon$.

In deriving (4), we assumed that the cloud optical properties (e.g., volume extinction, volume scatter and the scattering phase function) vary only with depth. This assumption is also applied to the source term and, for thermal emission, we consider the temperature of the medium to be independent of the horizontal location variables (u, v). The source term in (4) can therefore be written as[1]

$$\mathbb{N}_\epsilon = a(y)B(T)\mathbb{Z} \quad (21)$$

where $B(T)$ in this context is the Planck black body emission at temperature T, $a(y)$ is the volume absorption coefficient $[a(y) = \alpha(y) - s(y)]$ and $\mathbb{Z}$ is the vector

$$\mathbb{Z} = [1, 0, 0 \cdots]^T. \quad (22)$$

b. Side radiance amplitude term

We will assume here, only for reasons of simplicity, that the medium is uniformly illuminated equally on each of its vertical sides by the radiance $N_s(\mu)$. The general expression for the incident radiance amplitudes is (Eq. (31) of Part 1)

$$\hat{N}_{si,k}(l, w, y, \mu, a) = \frac{\eta}{(1 + \delta_a\delta_{k-1})\pi} \times \sum_{a'=0}^{\infty} \left\{[N_{l,1} + N_{l,1}^W(-1)^{w+a'+a}]F_{L,1k}W_w^{-1} + [N_{w,1} + N_{w,2}(-1)^{l+a'+a}]F_{W,1k}L_l^{-1}\right\}, \quad (23)$$

where l, w, $a = 0, 1, 2 \cdots$ and $0 \leq \eta \leq 1$ and the angular functions $F_{L,jk}$ and $F_{W,jk}$ are defined in the Appendix of Part 1. Since each side of the box is illuminated equally, we will consider here for the purpose of illustration only the incident radiance components on the west face of the box in detail. For this case

[1] We have assumed for convenience only that temperature and therefore $B(T)$ are independent of u and v. Horizontal variations in $B(T)$ can be incorporated by deriving an alternate form for $\hat{Z}$ using (1).

$$N_{w,1} = \frac{1}{(1+\delta_a)\pi}\int_{-\pi/2}^{\pi/2}\frac{2}{L_l}\left[\int_0^W N(u=0, v, y, \mu, \phi)\cos\frac{w\pi v}{W}\,dv\right]\cos a\phi\, d\phi$$

$$N_{w,2} = \frac{1}{\pi}\left[\int_{-\pi/2}^{\pi/2}\int_0^W N(u=0, v, y, \mu, \phi)\cos\frac{w\pi v}{W}\,dv\right]\sin a\phi\, d\phi \qquad (24)$$

A simplification to (23) follows by setting $N(0, v, y, \mu, \phi) = N_s(\mu)$ and by employing only the azimuthally averaged component of the radiance (i.e., set $a = 0$),

$$N_{w,1} = \frac{\delta_a\delta_w}{(1+\delta_a)\pi}N_s(\mu) \quad \text{and} \quad N_{w,2} = 0. \qquad (25)$$

Similar expressions can be derived for $N_{l,1}$, $N^w_{l,1}$ and $N^L_{w,1}$. Thus for $a = 0$, the incident lateral radiance amplitudes on the west face of the box are

$$N_{si,1}(l, w, y, \mu, a=0) = \frac{\eta}{2\pi}N_s(\mu)\left(\frac{i_w\delta_l}{W_w}F_{L,1k} + \frac{i_l\delta_w}{L}F_{W,1k}\right), \qquad (26)$$

where

$$i_m = 1 + (-1)^m.$$

Thus, the vectors $\hat{\mathbf{N}}_\epsilon$ defined by (21) and $\hat{\mathbf{N}}_{si}$ with elements given by the amplitudes (26) are used in (9) after being transformed according to (10).

7. Results

a. *Emergent solar radiation fields from finite clouds*

The radiative transfer equation (17) with the solar source term (19) was solved using the standard doubling methods incorporating the algorithms detailed in the Appendix. The calculations presented below apply only to the azimuthally averaged radiance fields (i.e., $a = 0$) which is in keeping with the approximation (6) and the series in (1) were truncated with $NL = 3$ and $NW = 3$. It is assumed that the only source of incident radiation on the cloud is that associated with the collimated beam along the direction defined by μ_0. We use a Henyey–Greenstein phase function with an asymmetry parameter $g = 0.865$ and set $\omega_0 = 1$ as a means of defining the relevant optical properties typical of water clouds in the visible portion of the solar spectrum.

The upwelling flux through cloud top, normalized with respect to the total radiative energy received by the cloud, is shown in Fig. 4 as a function of the solar zenith angle factor μ_0 for clouds of varying horizontal extent. The dimensions of the cloud are specified on the diagram in terms of the trio of optical lengths (αL, αW, αH) where αL and αW refer to the horizontal optical dimensions of the cloud (in the west–east and north–south directions) while αH is the cloud optical depth. The plane parallel limit is also shown on the diagram together with the Monte Carlo results of Davies (1978) which are depicted as discrete points. Fig. 4 serves to illustrate that, at least for $\mu_0 = 1$ and $\mu_0 = 0.5$, the multimode solution agrees well with the Monte Carlo results and that the solution tends to the standard plane parallel solution as L and W approach ∞. The diagram also highlights the large differences in the effect of sun angle on the scattered radiation from finite and infinite clouds (a point already discussed by Davies, among others).

It is instructive to evaluate the effects of cloud geometry on the radiance field by simulating the radiance detected by a satellite instrument. Fig. 5 shows a schematic of the field of view of such a detector which is large enough to contain the whole cloud but is not able to distinguish cloud top and side. The detector responds only to cloud top when looking vertically down and receives increasingly more contributions from the side as the viewing zenith angle increases. The radiance sensed by such a detector is shown in Figs. 6a and b as a function of the viewing angle as the detector scans through 90 degrees from the solar and antisolar sides to cloud top. Also shown on the diagrams are the appropriate radiance distributions determined for the plane parallel cloud with the same optical depth. The differences between plane parallel and finite theory apparent in Fig. 4 are again evident in the comparisons shown in Figs. 6a and b and highlight the problems associated with the interpretation

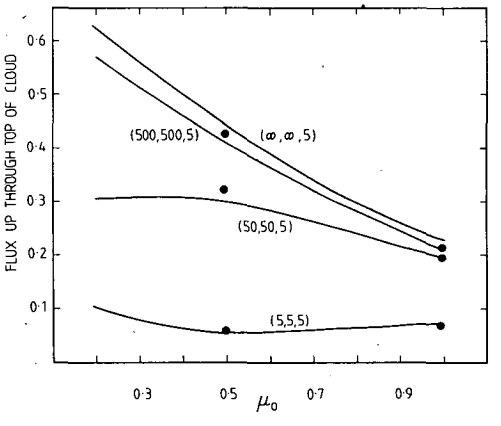

FIG. 4. Azimuthally and surface averaged emergent fluxes from cloud top as a function of solar zenith angle μ_0 for clouds of varying horizontal extent. The discrete points represent equivalent Monte Carlo solutions (from Davies, 1978).

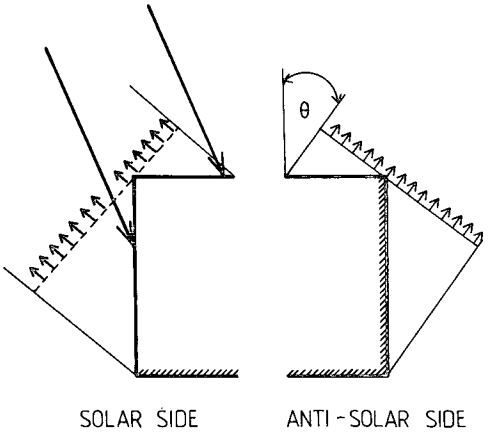

FIG. 5. Schematic view of the azimuthally averaged radiance detected by a radiometer that scans over the solar and anti-solar sides of the cloud.

of the radiances scattered from small clouds using plane parallel theory.

b. The transfer of infrared radiation in a finite cloud

The multimode radiative transfer equation (9) was solved in the manner discussed above with the source and side radiance terms given by (21) and (26) respectively and transformed according to (10). Only the azimuthally averaged radiances and irradiances are presented here and the series in (1) were truncated with $NL = 3$ and $NW = 3$. The cuboidal cloud was illuminated uniformly on its base from the ground below and equally on each of its vertical sides by a specified side radiance N_s. We again employ a Henyey–Greenstein phase function and, for the purpose of later comparison, we set $\omega_0 = 0.638$ and g (the asymmetry parameter) = 0.865 which are representative of a C-1 water cloud at 10 μm (Diermendjian, 1969).

1) COMPARISON WITH OTHER SOLUTIONS

The theoretical problem of infrared radiation transfer in finite clouds has recently been addressed in the work of Liou and Ou (1979) and Harshvardhan *et al.* (1981). We employ the work of the latter in the following comparisons since those authors include results of Monte Carlo computations and they also argue against the validity of the results of Liou and Ou (1979).

Comparisons between the results obtained from the solution of (8) and the Monte Carlo and two stream calculations of Harshvardhan *et al.* are shown in Fig. 7. The distributions shown on the diagram are of the hemispheric emergent fluxes from cloud top and side confined to the upward hemisphere. These flux distributions are expressed in terms of an equivalent black body temperature for a cloud with optical dimensions (10, 10, 10). To be consistent with Harshvardhan *et al.*, the solutions were obtained for a cloud illuminated isotropically from below on both the cloud base and sides. The particular case illustrated is for an isothermal cloud at 250 K above a black background of 300 K. Also shown are the surface averaged black body temperatures which represent the total flow of radiation from the respective sides of the cloud.

From the comparisons shown in Fig. 7, the broad features of top and side flux distributions are well represented by the multimode solutions while the two stream solutions of Harshvardhan *et al.* deviate significantly from the Monte Carlo solution.

2) DISTRIBUTED INCIDENT SIDE RADIANCES

The imposition of isotropic radiation incident on the sides of the cloud is an oversimplification in terms

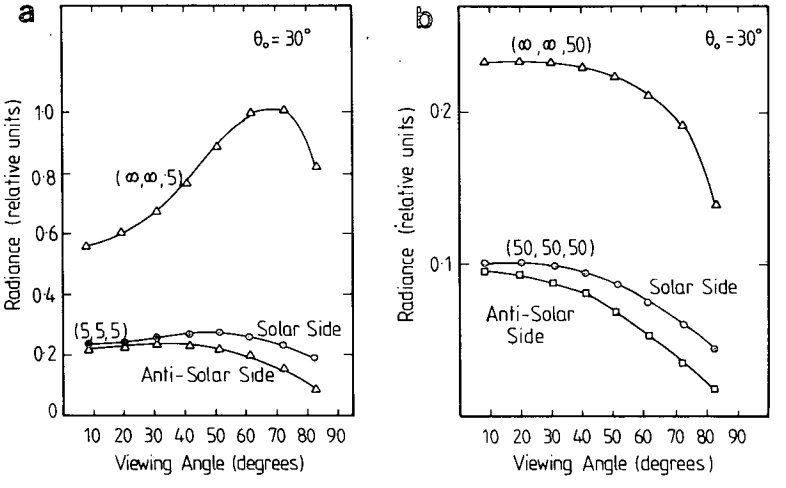

FIG. 6. Radiances as seen by the detector shown in Fig. 5 as a function of viewing angle θ for a cuboidal cloud with the given optical thickness (a) $\tau = 5$ and (b) $\tau = 50$.

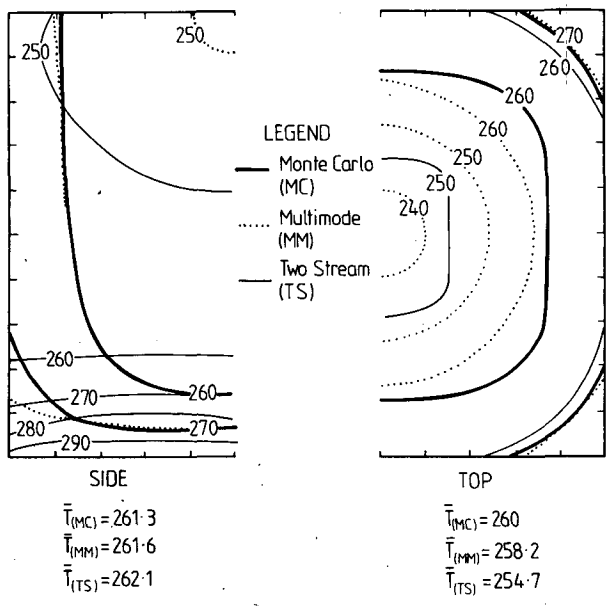

FIG. 7. Comparison between the two stream (thin), Monte Carlo (solid) and multimode solutions (dotted) of emergent upward hemispheric flux through the sides and top of a cuboidal cloud with $\tau = 10$. Also shown are the surface averaged equivalent temperatures for each solution.

of realistically modelling the incident side radiances. In reality, weak absorption such as that in the atmospheric window region of the IR absorption spectrum will produce anisotropic radiance fields. The following expression for N_s is employed in part as an attempt to include a more realistic angular distribution of incoming radiance. We set

$$N_s(\mu) = N_g \cos(\theta/2), \tag{27}$$

where N_g is the radiance associated with the emission from the ground. For θ ($= \cos^{-1}\mu$) measured from the vertical in the upward direction, N_s according to (26) varies from N_g for vertical radiances incident on the cloud base to zero incident radiance on the cloud top.

The flux distributions on the top and sides of the cloud were determined from the solution of the radiative transfer equation (8) upon substitution of (27) in the side radiance term (25). These distributions, shown in Fig. 8 as equivalent black body temperatures, were calculated for an isothermal cloud at 250 K over a black surface at 300 K. Superimposed on these contours are the distributions taken from Fig. 7. It is apparent from the comparison of these distributions that the angular variation of incident radiance on the sides of the cloud tends to smooth the flux distributions by suppressing the edge brightening effect. The average temperatures included in the diagram attest to the fact that mean flow of radiation through the sides of the cloud is significantly smaller for the case with distributed side radiances than for isotropic side radiances.

3) NON-ISOTHERMAL CLOUDS

The above calculations assume that the cloud is isothermal. It is more realistic to consider a cloud which is vertically stratified in temperature. To illustrate the versatility of the multimode procedure for this case, a cuboidal cloud of optical depth $\tau = 10$ was considered. The cloud top temperature for all computations was maintained at 250 K and the cloud base temperature was determined given the temperature difference ΔT between cloud top and base and the temperature of the ground beneath the cloud was fixed at 300 K. It was assumed that the Planck black body function varies as a linear function of optical depth and thus the source doubling relations of Wiscombe (1976a,b) were employed. For small ΔT, the variation of temperature from cloud base is then approximately linear. The impact of this temperature stratification on the distribution of upward hemispheric flux and on the surfaced averaged flux (shown as an equivalent temperature) is substantial according to Fig. 9. The simple isothermal assumption is evidently not applicable for problems that require a simulation of radiances from thick convective clouds that possess large values of ΔT.

4) THE NET IR BUDGET OF A CUBOIDAL CLOUD

The net gain or loss of IR radiation by a cloud, measured in terms of a net flux divergence, produces a radiative heating or cooling of the cloud layer itself. It was demonstrated by Stephens (1978) that the bulk of this cooling and heating occurs in the atmospheric window region of the absorption spectrum. Therefore the following results for 10 μm radiation can be con-

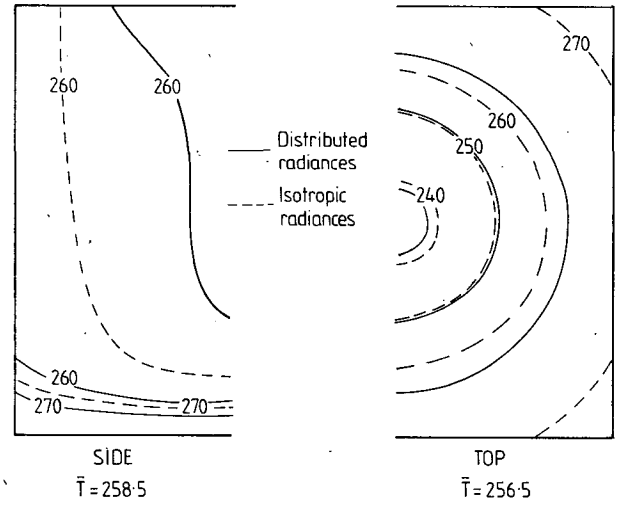

FIG. 8. Comparison between the upward hemispheric flux distributions for a cuboidal cloud illuminated by isotropic and by a distributed radiance field (see text). All other properties are as for Fig. 7.

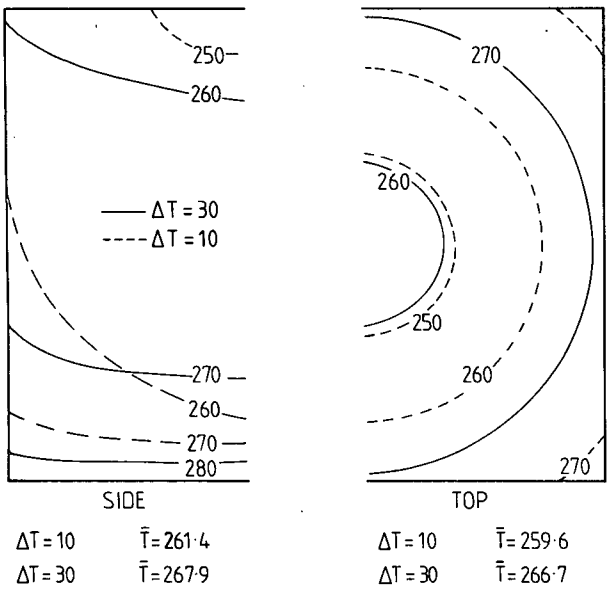

FIG. 9. Upward hemispheric flux distributions for nonisothermal clouds with a temperature variation from base to top defined by ΔT. All other properties are as for Fig. 7.

sidered as representative of the total broadband characteristics of the cloud.

Figure 10 presents the IR radiation budget of a cuboidal cloud as a function of cloud depth. The diagram shows the net loss and gain of IR radiation by the entire cloud normalized by the upward flux incident on the cloud base for two isothermal clouds at 250 and 280 over a 300 K black surface. The dashed curves illustrate the contribution to the total radiation budget from the combined loss through the four vertical sides of the cloud. Also shown are the net radiation budgets of plane parallel clouds with the same temperatures and optical depths. The comparison between the total radiative gain and loss by cuboidal clouds and plane parallel clouds demonstrates the importance of the exchange of radiation through the vertical sides of the cloud.

The cloud at a temperature of 280 K and optical thickness of 10 is perhaps typical of smaller cumulus clouds that are predominant in the lower tropical atmosphere. The results shown in Fig. 10 imply that the enhanced cooling effect (i.e., radiative loss) of finite cloud may play an important role in the stabilization of the lower tropical troposphere that, hitherto, has been underestimated on the basis of plane parallel theory.

8. Conclusions

The multimode radiative transfer equation derived in Part 1 was extended in this paper to include the source terms that characterize i) the diffuse radiance that results from the single scatter of a (collimated) beam directly transmitted to the given point within the medium, and ii) thermal emission within the medium. Thus the major objective of this paper was to extend the theories of Part 1 in a way that allows the multimode method to be applied to a number of problems typically encountered in studies of atmospheric radiation–cloud interaction.

The solutions of the multimode equation with the derived source terms were used to illustrate certain IR and solar radiative characteristics of hypothetical box shaped clouds. The results reiterate the findings of others (e.g., Davies (1978), McKee and Cox (1974), and Harshvardhan *et al.* (1981) and illustrate the importance of the exchange of radiative energy through the sides of clouds. In particular, the role of cloud shape on the interpretation of satellite radiances and on the IR radiative budget of a finite cloud has been studied.

When possible, the solutions were compared with available Monte Carlo results and the relatively close agreement between the two forms of solution support the contention that the multimode method is a viable and accurate solution to the general problem of anisotropic scattering in horizontally finite media. The computational effort required to obtain the solutions is comparable to that required to solve an equivalent plane parallel problem given the transformations discussed in Section 3 and the doubling algorithms derived in the Appendix. Advantages of the method, other than those already described in Part 1, are that the user is not forced to impose angular restraints on the incident and emergent radiance fields and that, in principle, detailed scattering phase functions can be incorporated in the solutions. Another advantage of the method, but not exploited in either Part 1 or the present study, is that the solutions are not restricted to provide only azimuthally averaged quantities.

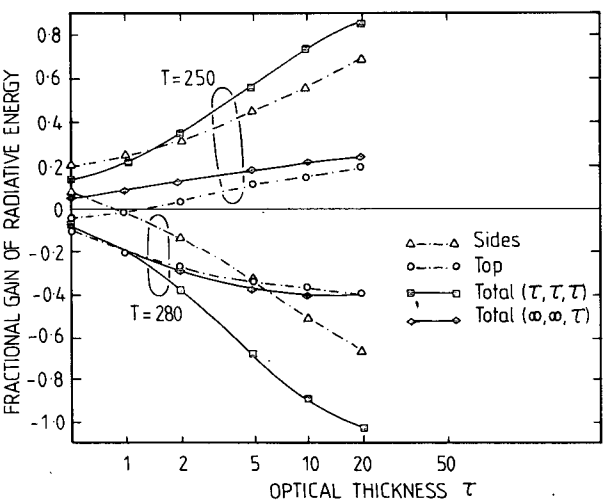

FIG. 10. The fractional net gain and loss of IR radiant energy for isothermal cuboidal and infinite clouds. Also shown are the respective fractional losses and gains by the various faces of the cuboidal cloud.

APPENDIX

Doubling Algorithms for Spatially Nonlinear Sources

The azimuthally averaged source function associated with the direct beam solutions for a box shaped medium can be represented by the amplitude

$$\hat{N}_\epsilon(l, w, y, \mu, a) = \frac{\omega_0}{4\pi}\bar{p}(\mu, \mu_0)\hat{N}_0(l, w, y, \mu_0, \phi_0), \quad \text{(A1)}$$

where $\bar{p}(\mu, \mu_0)$ is the azimuthally averaged phase function, ω_0 the single scatter albedo and $\hat{N}_0(l, w, y, \mu_0, \phi_0)$ is the radiance amplitude as obtained from the solutions (15) and (16). It is a relatively straightforward task to demonstrate that (A1) with (15) and (16) tend to the more familiar Beer's formula as $L \to \infty$.

1. General theory

The general theory for the inclusion of spatially nonhomogeneous source terms in the solution of the radiative transfer equation was developed by Grant and Hunt (1969). The underlying concept is to define the source, reflection and transmission functions for a thin layer and then build these up by the addition of sublayers. If we denote $\Sigma^+_{0,2^n}$ as the source vector associated with a layer $2^n\Delta\tau$ thick, then the source vector corresponding to the n addition of a layer $2^n\Delta\tau$ thick is

$$\left.\begin{aligned}\Sigma^+_{0,2^{n+1}} &= \mathbf{t}_n\Gamma_n(\mathbf{r}_n\Sigma^-_{2^n,2^{n+1}} + \Sigma^+_{0,2^n}) + \Sigma^+_{2^n,2^{n+1}}\\ \Sigma^-_{0,2^{n+1}} &= \mathbf{t}_n\Gamma_n(\mathbf{r}_n\Sigma^+_{0,2^n} + \Sigma^-_{2^n,2^{n+1}}) + \Sigma^-_{0,2^n}\end{aligned}\right\}, \quad \text{(A2)}$$

where $\mathbf{r}_n$ and $\mathbf{t}_n$ refer to the reflection and transmission matrices of a slab of n layers that comprise a thickness of $2^n\Delta\tau$ and obey the usual doubling rules while Γ_n is the propagator $[\Gamma_n = (I - r_n r_n)^{-1}]$. The relation between $\mathbf{r}_n$, $\mathbf{t}_n$ and the local matrices $\rho(y)$ and $\mathbf{t}(y)$ [see (18)] has been discussed in some length by Wiscombe (1976a) in the plane parallel context. One of the concerns of the present derivation is to relate the vectors $\Sigma^\pm_{0,2^n}$ to amplitudes $\hat{N}_\epsilon$.

For strictly nonhomogeneous sources, the above formula must be applied 2^n times to construct source functions for a layer $2^n\Delta\tau$ thick. On the other hand, homogeneous sources imply that

$$\Sigma^\pm_{2^n,2^{n+1}} = \Sigma^\pm_{0,2^n} \quad \text{(A3)}$$

and require only n cycles through (A2) to construct functions for layers $2^n\Delta\tau$ thick. Thus the requirement of the present derivation is to transform the source terms $\Sigma^\pm_{2^n,2^{n+1}}$ to a form containing $\Sigma^\pm_{0,2^n}$ in order to render (A2) in the form of doubling formulae.

2. Inhomogeneous source functions

We can factor the source functions defined by (15) and (16) substituted into (A1) in terms of its angular (μ) and spatial (τ) components by

$$\hat{N}_\epsilon(l, w, y, \mu, a = 0) = \bar{m}(\mu)\hat{s}(\tau) \quad \text{(A4)}$$

where, for our purposes, the $\hat{s}$ factor takes the form

$$\hat{s}_1(\tau) = a_1 e^{-\tau/\mu_0} - b_1\tau e^{-\tau/\mu_0} + c_1, \quad \text{(A5)}$$

$$\hat{s}_2(\tau) = e^{-\tau/\mu_0}\{(a_2 - d)\sin l'\tau - b_2\cos l'\tau\} + b_2, \quad \text{(A6)}$$

with

$$\begin{aligned} a_1 &= L - \sin\theta_0/\alpha\\ b_1 &= \tan\theta_0/\alpha\\ c_1 &= \sin\theta_0/\alpha\\ a_2 &= l\pi/(L\beta)\\ b_2 &= \frac{\alpha}{\sin\theta_0\beta}\\ l' &= \frac{l\pi}{L\alpha}\tan\theta_0\\ d &= L/l\pi\\ \beta &= \frac{\alpha^2}{\sin^2\theta_0} + \frac{l^2\pi^2}{L^2}. \end{aligned}$$

The thin layer $(i\Delta\tau, (i+1)\Delta\tau)$ source vector is defined by

$$\Sigma^\pm_{i,i+1} = S_i\Sigma^\pm_{in}, \quad \text{(A7)}$$

where

$$S_i = \frac{1}{\Delta\tau}\int_{i\Delta\tau}^{(i+1)\Delta\tau} s(\tau)d\tau, \quad \text{(A8)}$$

$$\Sigma^\pm_{in} = \mathbf{A}\begin{pmatrix}\bar{m}(\pm\mu_1)\\ \bar{m}(\pm\mu_m)\end{pmatrix} + \mathbf{B}\begin{pmatrix}\bar{m}(\pm\mu_1)\\ \bar{m}(\pm\mu_m)\end{pmatrix}.$$

The form of the **A** and **B** matrices depends only on the choice of the initialization scheme (e.g., Wiscombe, 1976a). For the sake of this study, these matrices can remain undefined.

It was demonstrated by Wiscombe (1976b) that the source vectors obey

$$\Sigma^\pm_{i,i+2^n} = \sum_{k=1}^{2^n} S_{k+i-1}\mathbf{V}^\pm_{k,n}, \quad \text{(A9)}$$

where the $\mathbf{V}^\pm_{k,n}$ vectors are independent of the spatial variable τ and depend only on the previous $\mathbf{V}^\pm_{k-1,n}$ vectors and, ultimately on the reflection and transmission functions for the thin $\Delta\tau$ slabs.

Thus (A9) can be manipulated to provide the relationship between $\Sigma^\pm_{2^n,2^{n+1}}$ and $\Sigma^\pm_{0,2^n}$ that is required to transform (A2) to a doubling rule.

a. *The $\hat{s}_1(\tau)$ source functions*

By substituting (A5) into (A8) and omitting the homogeneous (i.e., c_1) term we derive

$$\begin{aligned}\hat{s}_i(\Delta\tau) &= \frac{1}{\Delta\tau}\int_{i\Delta\tau}^{(i+1)\Delta\tau}(ae^{-\tau/\mu_0} - b\tau e^{-\tau/\mu_0})d\tau\\ &= \frac{\mu_0}{\Delta\tau}(q_1 e_i + p_1 e_i g_i), \end{aligned} \quad \text{(A10)}$$

where we adopt the notation "e_i" for "$e^{-i\Delta\tau/\mu_0}$" and "g_i" for "$i\Delta\tau$" and

$$\left.\begin{aligned} q_1 &= (a_1 + b_1)(e_1 - 1) - be_1g_1 \\ p_1 &= b_1(e_1 - 1) \end{aligned}\right\}. \quad \text{(A11)}$$

Thus (A9) becomes

$$\Sigma^{\pm}_{2^n,2^{n+1}} = \sum_{k=1}^{2^n} (e_{k-1+2^n}q_1 + e_{k-1+2^n}g_{k-1+2^n}p_1)V^{\pm}_{k,n}$$

$$= e_{2^n}\Big(\sum_{k=1}^{2^n} (e_{k-1}q_1 + e_{k-1}g_{k-1}p_1) \times V^{\pm}_{k,n} + e_{k-1}g_{2^n}p_1y^{\pm}_{0,2^n}\Big), \quad \text{(A12)}$$

where

$$y^{\pm}_{2^n} = \sum_{k=1}^{2^n} e_{k-1}V^{\pm}_{k,n}.$$

The summation on the right-hand side of (A12) is simply $\sum^{\pm}_{0,2^n}$ with $i = 0$ and the $y^{\pm}_{2^n}$ vectors are those associated with the exponential in τ source functions for which the doubling relations of Wiscombe (1976b) apply. That is

$$\left.\begin{aligned} y^{+}_{2^{n+1}} &= t_n\Gamma_n(e_{2^n}r_ny^{-}_{2^n} + y^{+}_{2^n}) + e_ny^{+}_{2^n} \\ y^{-}_{2^n} &= t_n\Gamma_n(r_ny^{+}_{2^n} + e_ny^{-}_{2^n}) + y^{-}_{2^n} \end{aligned}\right\}. \quad \text{(A13)}$$

Therefore the doubling relationships for the source functions which have an $\hat{s}_1(\tau)$ optical thickness dependence can be written as

$$\left.\begin{aligned} \Sigma^{+}_{0,2^{n+1}} &= t_n\Gamma_n(r_ne_{2^n}\Sigma^{-}_{0,2^n} + e_ng_{2^n}p_1y^{-}_{2^n}) + e_{2^n}\Sigma^{+}_{0,2^n} + e_{2^n}g_{2^n}p_1y^{+}_{2^n} \\ \Sigma^{-}_{0,2^{n+1}} &= t_n\Gamma_n(r_n\Sigma^{+}_{0,2^n} + e_{2^n}\Sigma^{-}_{0,2^n} + e_{2^n}g_{2^n}p_1y^{-}_{2^n}) + \Sigma^{-}_{0,2^n} \end{aligned}\right\}. \quad \text{(A14)}$$

b. The $\hat{s}_2(\tau)$ source functions

For this case, (A6) substituted in (A8) produces (again we omit the homogeneous term)

$$\hat{s}_i(\Delta\tau) = e_i(p_2s_i + q_2c_i) \quad \text{(A15)}$$

with

$$p_2 = a'(e_1c_1 - 1) - b'e_1s_1$$

$$q_2 = b'(e_1c_1 - 1) + a'e_1s_1$$

$$s_i = \sin l'i\Delta\tau$$

$$c_i = \cos l'i\Delta\tau$$

and

$$a' = -\frac{a+d}{\mu_0\gamma} - \frac{bl'}{\gamma}$$

$$b' = -\frac{l'(a-d)}{\gamma} + \frac{b}{\mu_0\gamma}$$

$$\gamma = \frac{1}{\mu_0^2} + l'^2.$$

Eq. (A9) for $\Sigma^{\pm}_{2^n,2^{n+1}}$ becomes

$$\Sigma^{\pm}_{2^n,2^{n+1}} = \sum_{k=1}^{2^n} e_{k+2^n-1}(s_{k-1+2^n}p_2 + q_2c_{k+2^{n-1}})v^{\pm}_{k,n}, \quad \text{(A16)}$$

and by separating the sine and cosine terms we write

$$\left.\begin{aligned} \Sigma^{\pm}_{2^n,2^{n+1},1} &= \sum_{k=1}^{2^n} e_{k-1+2^n}q_2c_{k+2^{n-1}}v^{\pm}_{k,n} \\ \Sigma^{\pm}_{2^n,2^{n+1},2} &= \sum_{k=1}^{2^n} e_{k-1+2^n}p_2s_{k+2^{n-1}}v^{\pm}_{k,n} \end{aligned}\right\}. \quad \text{(A17)}$$

Then it can be simply demonstrated that

$$\left.\begin{aligned} \Sigma^{\pm}_{2^n,2^{n+1},1} &= e_{2^n}c_{2^n}\Sigma^{\pm}_{0,2^n,1} - \left(\frac{q_2}{p_2}\right)e_{2^n}s_{2^n}\Sigma^{\pm}_{0,2^n,2} \\ \Sigma^{\pm}_{2^n,2^{n+1},2} &= e_{2^n}c_{2^n}\Sigma^{\pm}_{0,2^n,2} + \left(\frac{p_2}{q_2}\right)e_{2^n}s_{2^n}\Sigma^{\pm}_{0,2^n,1} \end{aligned}\right\}. \quad \text{(A18)}$$

Thus (A18) can be directly substituted in the general formulas (A2) to provide doubling formula for $\Sigma^{\pm}_{0,2^{n+1},j}$ (where $j = 1, 2$) and it follows that

$$\Sigma^{\pm}_{0,2^{n+1}} = \Sigma^{\pm}_{0,2^{n+1},1} + \Sigma^{\pm}_{0,2^{n+1},2}. \quad \text{(A19)}$$

REFERENCES

Davies, R., 1978: The effect of finite geometry on the three-dimensional transfer of solar irradiance in clouds. *J. Atmos. Sci.*, **35**, 1712–1724.

Deirmendjian, D., 1969: *Electromagnetic Scattering on Spherical Polydispersions.* Elsevier, 290 pp.

Grant, I., and G. E. Hunt, 1969: Discrete space theory of radiative transfer I. Fundamentals. *Proc. Roy. Soc. London,* **A313**, 183–197.

Harshvardhan, J. A. Weinman and R. Davies, 1981: Transport of infrared radiation on cuboidal clouds. *J. Atmos. Sci.*, **38**, 2500–2513.

Liou, K. N., and S. C. Ou, 1979: Infrared radiative transfer in finite cloud layers. *J. Atmos. Sci.*, **36**, 1985–1996.

McKee, T. B., and S. K. Cox, 1974: Scattering of visible radiation by finite clouds. *J. Atmos. Sci.*, **31**, 1885–1892.

Preisendorfer, R. W., and G. L. Stephens, 1984: Multimode radiative transfer in finite optical media. I: Fundamentals. *J. Atmos. Sci.*, **41**, 709–724.

Stephens, G. L., 1978: Radiative properties of extended water clouds. Part I. Theory. *J. Atmos. Sci.*, **37**, 2112–2123.

Van de Hulst, H. C. 1980: *Multiple Light Scattering, Tables, Formulae and Application,* Vol. 1, Academic Press, 299.

Wiscombe, W., 1976a: On initialization, error, and flux conservation in the doubling method. *J. Quant. Spectrosc. Radiat. Transfer,* **16**, 637–658.

——, 1976b: Extension of the doubling method to inhomogeneous sources. *J. Quant. Spectrosc. Radiat. Transfer,* **16**, 477–489.